Supplemental Information

Neural Circuit Mechanisms for Pattern Detection and Feature Combination in Olfactory Cortex

Ian G. Davison and Michael D. Ehlers
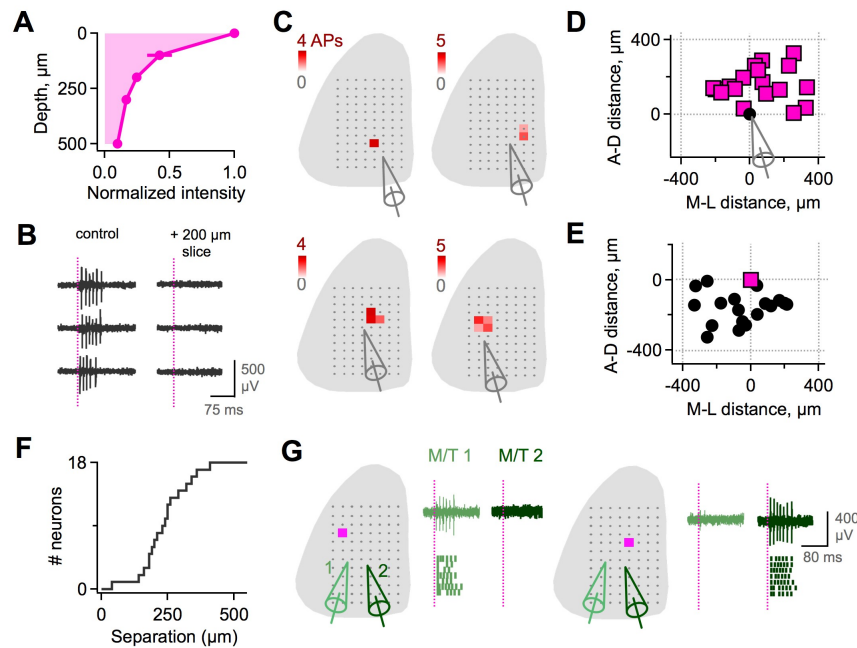
Supplemental Data

Figure S1, related to Figure 1. Characterization of MOB Responses to Photostimulation.

(A) Penetration of the UV uncaging beam in MOB tissue. Acute brain slices of varying thickness were cut from MOB and inserted in the UV beam path, and attenuation was measured with a power meter (Newport). Power dropped off rapidly in the first ~150 µm of tissue, suggesting that glutamate release was largely confined to superficial MOB layers where M/T apical dendrites are segregated within glomeruli.

(B) Effective depth of *in vivo* photostimulation of MOB. M/T firing driven by uncaging was largely blocked by overlaying a 200 µm brain slice of MOB (from a second animal) on the uncaging region during extracellular recordings.

(C) Examples of typical MOB 'output maps' illustrating the resolution provided by uncaging. Intensity shows the mean M/T spike count generated by each scan grid location. M/T firing was driven by 1-4 neighboring sites on the dorsal MOB surface (mean = 2.2). Pipettes illustrate position of electrode tip for each recording. APs, action potentials; grid spacing, 100 µm.

(D) Relative positions of the most effective uncaging site for each M/T (magenta squares), aligned to the corresponding recording electrode location (black circle; n = 18 M/Ts). Maximally effective sites rarely coincided with the electrode tip, further suggesting that M/Ts

were driven by activation of their superficial dendritic tufts rather than their soma. Effective sites were confined to a radius of ~300-400 μm from the electrode tip, consistent with connectivity between M/T somata and apical dendrites within glomeruli. A-D, anterodorsal; M-L, mediolateral.

(E) Data from (D) replotted to show recording positions (black) aligned to the maximal uncaging site (magenta).   Uncaging drove activity in a spatially dispersed population of M/Ts that was nonetheless confined to a ~300-400 μm radius around the photostimulation site.

(F) Cumulative plot of separation between recording location and most effective uncaging site for all recorded M/Ts.

(G) Example simultaneous recording from two M/Ts, showing that uncaging independently activates cells contained within different glomeruli. Pipettes (1) and (2) indicate positions of each electrode tip. Traces and rasters (right) show uncaging responses for the site indicated on the MOB map (left).
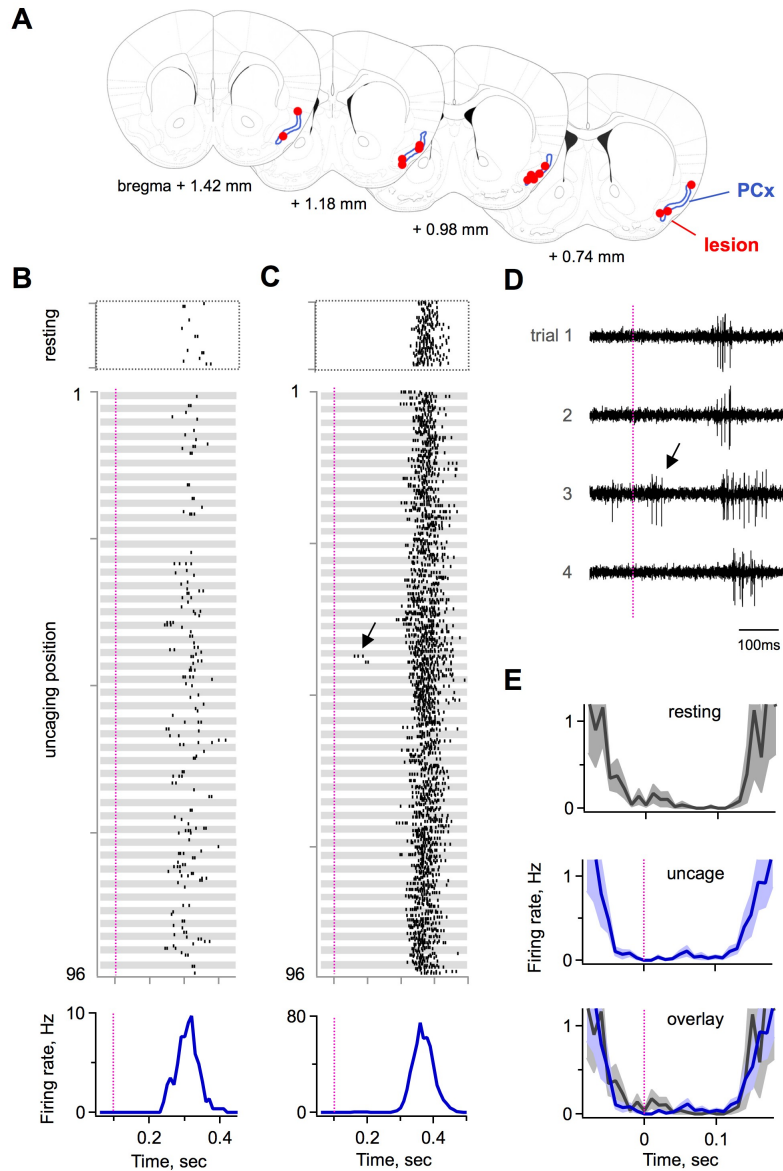
Figure S2, related to Figure 2. PCx Neuron Responses to Single-Site Uncaging in MOB.

(A) Subset of extracellular recording sites reconstructed from electrolytic lesions, superimposed on schematic atlas sections modified from (Paxinos, 2001).

(B) Single-site MOB photostimulation responses in an example PCx neuron, showing the full set of 96 photostimulated MOB positions (gray horizontal bars) each tested over 3 trials. Although the cell displayed consistent respiratory-coupled activity at rest (seen as spikes in the 250-400 msec time window), uncaging-evoked firing time-locked to UV delivery (magenta line) was completely absent.

(C) Scanning photostimulation for a second example PCx neuron, illustrating rare action potential responses. Two sites elicited firing in this cell, each on a single trial.

(D) Expanded view of the trials indicated by the arrowhead in (B), showing photostimulation response on one of four trials.

(E) Pooled data for all PCx neurons comparing firing rates for all unstimulated (gray, top) and uncaging (blue, center) trials. Bottom panel shows an overlay of the pooled data sets.
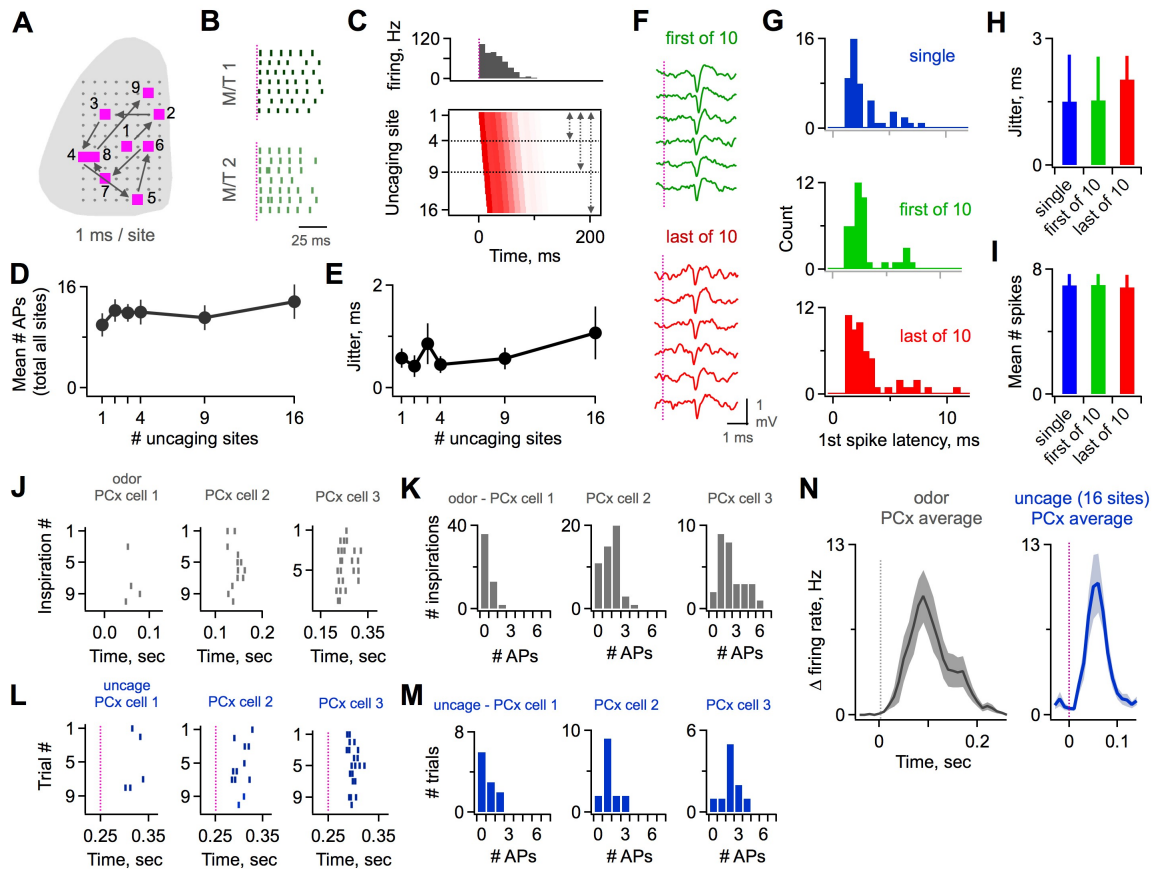
Figure S3, related to Figure 3. Multisite Photostimulation of MOB with Complex Patterns.

(A) Schematic of photostimulation with multisite uncaging patterns. Each site within a pattern was activated in rapid temporal sequence, 1 ms apart (0.5 ms uncaging pulse plus 0.5 ms repositioning time).

(B) Firing of two simultaneously recorded M/Ts during 2-site photostimulation (each M/T driven independently at different MOB locations; rasters show repeated trials; same neurons as depicted in Figure S1). Uncaging at effective sites for both neurons, 1 ms apart, produced spike trains that were highly overlapping other than a slight shift in onset (M/T 2 lags M/T 1).

(C) Predicted temporal profile of activity in a population of M/Ts driven with complex uncaging patterns. Top histogram, mean time course of M/T firing from single-site uncaging experiments as shown in Figure S1. Bottom plot shows this time course for M/Ts activated at different MOB positions in a multisite pattern, shifted according to position in uncaging sequence. Substantial overlap of M/T activity at different MOB locations is predicted even for larger patterns.

(D) Incorporating additional sites into uncaging patterns did not affect the total number of M/T spikes (summed across all scan sites; each site activated once and only once for both single site scanning and each set of patterns of different sizes), suggesting that photostimulation-evoked output from MOB was not substantially reconfigured by local circuits in these experiments. Uncaging patterns may have had minimal overlap with the sparse 'glomerular receptive fields' of each M/T (Fantana et al., 2008). Uncaging may also have driven M/Ts at the high end of their dynamic range, such that any lateral interactions generated little shift in their action potential output. M/T firing did not emerge for patterns lacking effective single-site uncaging locations (not shown).

(E) Additional uncaging sites also had little effect on the variability of M/T firing as assessed by jitter of initial spikes.

(F) Initial action potential firing for the same M/T tested at first and last positions in a 10-site uncaging sequence (green and red traces, respectively; 6 trials for each conditions; vertical line indicates delivery of uncaging pulse to this cell's effective MOB site).

(G) Histograms showing pooled latency data for 6 M/Ts tested at first and last positions in a 10-site sequence. Blue, single effective uncaging site. Green and red, M/Ts activated first and last in a sequence, respectively.

(H) Mean latency showed no significant difference in spike jitter when neurons were driven either first or last in a 10-site sequence ($p > 0.4$, t-test comparing first and last positions, $n = 6$ M/Ts). Bars show mean $\pm$ S.E.M. Colors as in (G).

(I) Mean spike count was also independent of position in an uncaging sequence ($p > 0.7$, t-test, $n = 6$ M/Ts). Colors shown as in (G).

(J) Representative odor-evoked firing in PCx neurons for weak (left), moderate (middle), and strong responses (right) in different neurons. Each row of the raster plot shows a single respiratory cycle taken from one odor presentation (4 s). Firing was reliable for strongly activated cells, but more variable across cycles and odor presentations for weakly activated cells.

(K) Histogram of spike counts for all respiratory cycles, corresponding to the neurons in (M) and including additional odor presentations.

(L, M) PCx neuron firing for multisite uncaging patterns (9-16 sites), shown for comparison with odor responses. Data presented as in (J) and (K). Firing was highly reliable for strongly activated cells, comparable to that seen with odor stimuli.

(N) Odor stimuli and 16-site uncaging patterns generate similar mean firing rates. Vertical line shows inspiration peak (odors) or UV pulse (uncaging). Odor responses have a more extended time course, potentially due to the more extended M/T spike trains produced by odor stimuli.
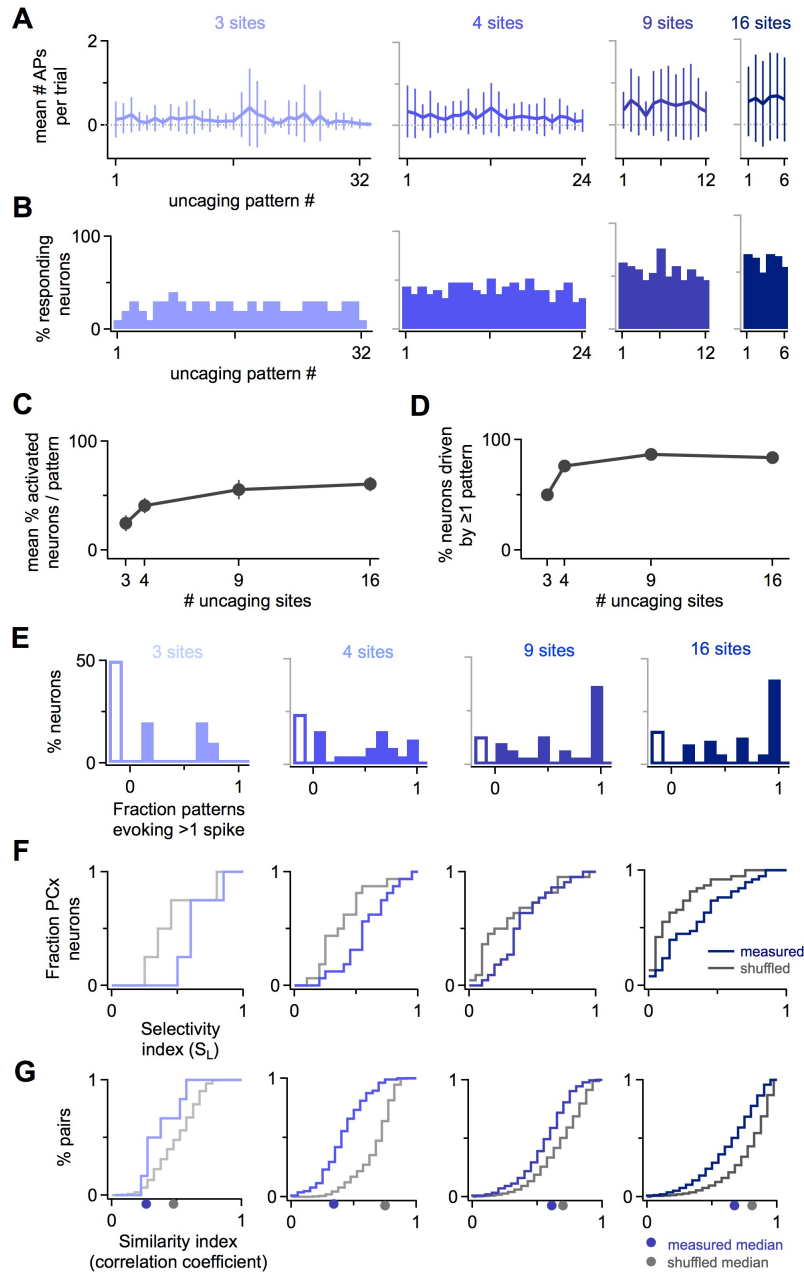
Figure S4, related to Figure 4. PCx Responses to Multisite Uncaging Patterns.

(A) Mean spike count evoked by each multisite pattern, averaged for all trials and all recorded cells. Mean counts are low for any given pattern because of cells that were either unresponsive overall or responded only to a subset of patterns. While PCx neurons preferred specific MOB patterns at the single neuron level (Figure 4), no pattern was more effective than others at the population level ($p > 0.9$; Kruskal-Wallis test). Error bars indicate $\pm$ SD.

(B) Fraction of PCx neurons activated by each of the multisite uncaging patterns in our test set. Any individual 3-site pattern drove only a relatively small proportion of cells; larger patterns were increasingly effective.

(C) Mean efficacy of multisite uncaging patterns of different sizes. On average, 9- or 16-site patterns drove on average >50% of PCx neurons.

(D) Uncaging efficacy measured as the fraction of neuron activated by ≥1 multisite stimulus, evaluated for each pattern size.

(E) Histogram showing the number of effective uncaging patterns for different PCx neurons. Open bars denote neurons unresponsive to any test pattern.

(F) Quantitative analysis of pattern detection. We calculated a selectivity index (lifetime sparseness, see Methods) for all cells that fired on >1 trial, using both original and shuffled data. Cumulative plots show that measured responses were consistently more selective across the set of stimulus patterns (blue) than predicted by randomly shuffling each cell's dataset (gray).

(G) Analysis of pattern selectivity in different PCx neurons. Response profiles of each neuron were converted to a vector, and profiles of all neurons were compared in a pairwise manner by calculating correlation coefficients. Histogram shows the distribution of coefficients for measured (blue) and shuffled data (gray), indicating that different PCx neurons preferred different sets of MOB patterns. Distributions were significantly different for pattern of 4, 9, and 16 ($p \ll 0.01$; Kolmogorov-Smirnov test). Filled circles indicate medians.

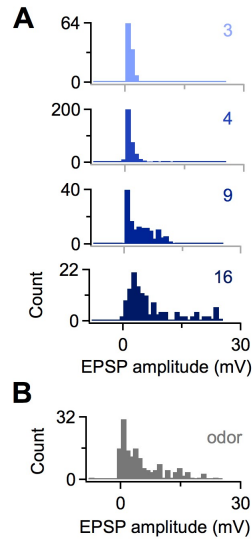**Figure S5, related to Figure 6.** EPSP Amplitudes Produced by Multisite Uncaging and Odors.

(A) Histograms of EPSP peak amplitudes in PCx neurons driven by multisite uncaging, shown for patterns of different sizes indicated by numbers at the right.

(B) Corresponding histograms of EPSP amplitudes for sensory stimulation. EPSPs for odor responses were on average smaller than responses to 16-site stimuli.

Supplemental Experimental Procedures

Rodent Surgery

Mice (C57Bl/6J, age 12-24 weeks, of both sexes) were anesthetised with a ketamine/dexdomitor mixture (i.p., 100/1 mg/kg) supplemented with atropine (0.2 mg/kg). The dorsal surface of the MOB was exposed via a craniotomy and the dura carefully removed to allow diffusion of MNI-caged glutamate into the brain. A second craniotomy was performed caudally to provide electrode access for recording from anterior piriform cortex. Anesthesia was transitioned to sevoflurane or isoflurane for recording of sensory-evoked or uncaging-evoked activity, respectively. All surgical procedures were in accordance with the guidelines of Duke University's Institutional Animal Care and Use Committee.

Odor Stimulation

The odorant test panel contained 13 odorant compounds with diverse chemical structures: propionic acid, isobutyraldehyde, geraniol, methyl salicylate, guaiacol, citral, (+)-carvone, 2-pentyl furan, 1-pentanol, diethylamine, eugenol, amyl acetate, and limonene. All odorants were high purity, purchased from Sigma. Odorants were diluted in mineral oil (Sigma) according to vapor pressure to give a headspace concentration of 10 ppm. A constant airstream (charcoal-filtered O_2 + anesthetic, 1.8 L/min) was delivered to the animal, supplemented by the odor delivery line (0.2 L/min, carrying filtered O_2 between stimuli). Software triggers delivered the headspace from each odorant's vial via dedicated lines and solenoid valves to a manifold where odors joined the main O_2/anesthesia line, giving a further 10X flow dilution (0.2 L/min odorant flow into 1.8 L/min main flow). A second valve at this point provided final control over odorant delivery to the animal for a period of 4 s, switching between lines carrying clean deodorized flow and the odorant headspace.

Electrophysiological Recordings

Recordings were targeted to anterior piriform cortex using stereotaxic coordinates (0.5-1.9 mm anterior to bregma; 2.0-3.2 mm lateral from midline for anterior and posterior locations repectively) based on (Paxinos, 2001). Electrodes were advanced through the caudal craniotomy at 45° to accommodate the scan objective. A subset of extracellular recording locations was

reconstructed using electrolytic lesions (Figure S2). Extracellular action potential waveforms were recorded with tungsten microelectrodes (2-4 MΩ, MicroProbes, Gaithersburg MD). Signals were amplified 10,000X and bandpass filtered from 500Hz – 5kHz (Model 1800, A-M Systems, Carlsborg, WA). Well-isolated single units were identified using a template-matching algorithm (Spike2, CED, Cambridge, England). Intracellular recordings were made with sharp electrodes (1.0 x 0.5 mm borosilicate glass, FHC, Bowdoinham ME, pulled to resistances 70-120 MΩ, filled with 3M potassium acetate). Membrane potential was amplified with an Axoclamp 2B (Molecular Devices, Sunnyvale CA). Data were acquired using either Spike2 software with Power1401 digitizer or with a DAQ board (PCI6035E, National Instruments, Austin TX) using custom software written in Igor Pro (Wavemetrics, Lake Oswego OR).

Glutamate Uncaging

The dorsal MOB was superfused with 2 mM MNI-caged glutamate (Tocris, Ellisvile MO) in ACSF (in mM: NaCl , KCl, CaCl$_2$, MgCl$_2$, D-glucose, HEPES,) and 0.5-0.6 ms uncaging pulses were delivered by Q-switching a 355 nm laser (DPSS 3500, Santa Clara CA) in combination with a mechanical shutter (Uniblitz, Rochester NY). ACSF was exchanged following each uncaging trial. Custom beam steering optics consisted of scan mirrors (Cambridge Technology 6510, Lexington MA), scan lens and tube lens (Edmund Optics), and a 5X objective (Carl Zeiss Inc.). Uncaging spot size was ~40 μm and uncaging locations were arranged in an 8x12 grid covering ~1 mm^2, corresponding to a large fraction (~70-80%) of the accessible dorsal MOB. Power at the brain surface was ~40 mW delivered to a total region of ~1200 μm^2, attenuated with neutral density filters to balance resolution and efficacy. UV penetration into the brain was ~150-200 μm, and M/Ts appeared to be activated via their apical dendrites in the glomerular layer, driving functionally related MOB neurons in accordance with the OR map (Figure S1). For multisite uncaging experiments, the uncaging spot was switched between successive positions in the scan pattern every 1 ms (Figure S3). Multisite patterns were constructed by randomly selecting of a set of uncaging sites, such that each of the 96 scan sites was activated once in each series of patterns. This produced a set of distributed stimuli that were qualitatively similar to the patterns of glomerular activity produced by odors (Rubin and Katz, 1999; Wachowiak and Cohen, 2001).

Data Analysis

Electrophysiological data were analyzed in time windows covering -100 ms to +400 ms relative to each inspiration peak (odor stimuli) or relative to the UV pulse (photostimulation experiments). Spike times were detected using Spike2 software followed by further analysis with custom Igor Pro routines. Response strength was quantified for both odors and uncaging by calculating peristimulus time histograms and/or firing rates using 10 ms bins, over either the full respiratory cycle (odors) or a 150 ms window following UV delivery (uncaging) that encompassed the M/T spike trains generated in MOB. Responses were averaged over all respiratory cycles during all odor presentations or over all trials for each uncaging stimulus. Changes in firing were either calculated as the difference from resting activity during prestimulus periods, or overlaid on resting activity for direct comparison. We also quantified responses using mean spike counts for each inspiration or uncaging trial, also as change in firing relative to resting activity. Intracellular data were analyzed similarly by averaging membrane potential over each inspiration or uncaging trial, computing EPSP integrals from averaged traces for both stimulus and resting trials, and calculating response strength as ($\int$EPSP$_{stimulus}$ − $\int$EPSP$_{prestimulus}$). Mean spike counts and EPSP integrals were used for further population analyses. Because synaptic input in PCx for single-site uncaging stimuli was small relative to ongoing respiratory-driven activity, we measured responses during periods of low background by delivering pulses between inspiration cycles (Figure 1). Synchronizing single-site uncaging pulses with respiratory-driven activity was also ineffective at driving firing in extracellularly recorded PCx neurons.

To test the selectivity of PCx firing across different MOB uncaging patterns, we calculated a lifetime sparseness index S_L for each neuron that quantified the degree to which it responded solely to a single stimulus ($S_L = 1$) versus equally to all stimuli ($S_L = 0$; (Davison and Katz, 2007). We assessed the significance of selectivity by shuffling each neuron's dataset, reassigning the spiking response on each trial to a randomly selected stimulus. The p-value for each neuron was derived from the distribution of 10,000 such permutations. Selectivity profiles for different neurons were compared by converting the response profile of each cell into a vector containing the mean spike count generated by each pattern, and calculating correlation coefficients for all possible pairs of neurons.

To construct maps of MOB output and PCx input, we averaged the responses at each location to several photostimulation trials (≥3 sites). MOB maps were displayed using mean spike counts at each uncaging site. For PCx synaptic input maps, we displayed sites that were classified as synaptically connected. This included sites where either integrated EPSP area or change in membrane potential exceeded ≥2 SDs of the fluctuations in unstimulated trials. Evoked EPSPs were also identified by visual inspection to avoid excluding responses below this threshold, and we required EPSPs to be present in >1 trial to avoid false positives resulting from ongoing activity.

Supplemental References

Davison, I.G., and Katz, L.C. (2007). Sparse and selective odor coding by mitral/tufted neurons in the main olfactory bulb. J Neurosci *27*, 2091-2101.

Fantana, A.L., Soucy, E.R., and Meister, M. (2008). Rat olfactory bulb mitral cells receive sparse glomerular inputs. Neuron *59*, 802-814.

Paxinos, G., and Franklin, K. B. J. (2001). The Mouse Brain in Stereotaxic Coordinates, 2nd edn (San Diego, CA: Academic Press).

Rubin, B.D., and Katz, L.C. (1999). Optical imaging of odorant representations in the mammalian olfactory bulb. Neuron *23*, 499-511.

Wachowiak, M., and Cohen, L.B. (2001). Representation of odorants by receptor neuron input to the mouse olfactory bulb. Neuron *32*, 723-735.